Principle in Imaging Contrast in Scanning Electron Microscopy for Binary Microstructures Composed of Organosilane Self-Assembled Monolayers

N. Saito,*,† Y. Wu,†,‡ K. Hayashi,† H. Sugimura,† and O. Takai†

Department of Materials Engineering, Graduate School of Engineering, Nagoya University, Furo-cho, Chikusa-ku, Nagoya 464-8603, Japan, and Aichi Science & Technology Foundation, Marunouchi 2-4-7, Naka-ku, Nagoya 460-0002, Japan

Received: June 6, 2002; In Final Form: November 6, 2002

Field-emission electron microscopy (FE-SEM) was applied to observe coplanar microstructures composed of two different types of organosilane self-assembled monolayers (SAMs). These binary microstructures were prepared on silicon substrates covered with native oxide by a lithographic technique. Four types of organosilane precursors, they are *n*-octadecyltrimethoxysilane (ODS), heptadecafluoro-1,1,2,2-tetrahydro-decyl-1-trimethoxysilane (a type of fluoroalkylsilane, FAS), *n*-(6-aminohexyl)aminopropyltrimethoxysilane (AHAPS), and 4-(chloromethyl)phenyltrimethoxysilane (CMPhS), were used in this study. Micropatterns composed of the SAMs were clearly imaged by FE-SEM at low acceleration voltages, around 0.6 kV. The brightness order of the SAMs in FE-SEM was ODS > AHAPS > CMPhS > FAS. Through ab initio molecular orbital calculations, the origin of this FE-SEM contrast was ascribed to the electron affinity between the SAMs, which governed the FE-SEM image contrast. It has been successfully demonstrated that FE-SEM could provide us chemical information on organic films with a monomolecular thickness on a solid support.

1. Introduction

Micropattering of the self-assembled monolayer (SAM) is an attractive technique to produce organic templates for various microfabrication processes including that for molecular electronic devices.[1−4] Observation of SAMs in micro/nano regions is crucial in order to develop the microfabrication processes. Micropattered SAMs have been mainly evaluated so far by scanning probe microscopy, e.g. lateral force microscopy (LFM),[5−7] Kelvin probe force microscopy (KPFM),[8−10] and so on. LFM and KPFM provide us surface friction and surface potential in micro/nano regions, respectively. Such chemical information has played an important role on the fabrication of microstructured SAMs. We have reported on surface potentials of organosilane SAMs on silicon substrates, which had been prepared from *n*-octadecyltrimethoxysilane [ODS:$H_3C(CH_2)_{17}$-$Si(OCH_3)_3$], heptadeca fluoro-1,1,2,2-tetrahydro-decyl-1-trimethoxysilane [a type of fluoroalkylsilane, FAS:$F_3C(CF_2)_7$-$(CH_2)_2Si(OCH_3)_3$], *n*-(6-amino-hexyl)aminopropyltrimethoxysilane [AHAPS:$H_2N(CH_2)_6NH(CH_2)_3Si(OCH_3)_3$], and 4-(chloromethyl)phenyltrimethoxysilane [CMPhS:$H_2ClC(C_6H_4)Si(OCH_3)_3$].[9,10] Relative surface potentials of FAS, AHAPS, and CMPhS−SAMs with the reference to ODS−SAM were ca. −170, +50, and −30mV, respectively, as measured by KPFM. Thus the order of surface potential is as follows:

$$\text{AHAPS-SAM} > \text{ODS}-\text{SAM} > \text{CMPhS}-\text{SAM} > \text{FAS}-\text{SAM} \quad (1)$$

The surface potential deference between SAM1 and SAM2 is explained by the following equation:

$$\Delta V_{\text{SAMvs.SAM2}} = -\{\Phi(\text{SAM1}) - \Phi(\text{SAM2})\}/e \quad (2)$$

where the $\Phi(i)$ and e are the work function of component i and proton charge, respectively. Thus, the surface potentials are determined by the differences in the Fermi levels of the SAMs.

Bittermann et al. observed Langmuir−Blodett films on silicon substrates by field-emission scanning electron microscopy (FE-SEM) without a metal overcoating on the films.[11] They found that FE-SEM contrasts appeared in the film through the distribution of molecular packing density. However, they have not studied FE-SEM contrast between films composed of different types of molecules.

In this investigation, micropatterned binary SAMs have been observed by FE-SEM. These microstructures are prepared from organosilane precursors on silicon substrates covered with native oxide. The acquired FE-SEM contrasts are studied by comparing the contrasts with corresponding surface potential contrasts acquired by KPFM. Furthermore, because the FE-SEM contrasts are considered to be closely related to electronic structures of the SAMs, the principle of the image contrast is discussed from the viewpoint of the electronic structures of the SAMs estimated by ab initio molecular orbital (MO) calculations.

2. Experiments

2.1. Preparation and Patterning of SAM. ODS, FAS, CMPhS, and AHAPS−SAMs were prepared on the substrates of n-type silicon (100) by a vapor phase method.[12,13] Figure 1 depicts the process from preparation to patterning. In step 1, a silicon substrate surface covered with a thin oxide layer (ca. 2 nm) was cleaned and hydroxylated simultaneously by a UV/ozone cleaning method. The light source was an excimer lamp with $\lambda = 172$ nm and 10 mW/cm^2 (Ushio Electric, UER20−172V). In step 2, a SAM was deposited on the substrates. In step 3, the substrate surface was irradiated under a reduced pressure of 10 Pa with excimer lamp through a photomask. In this step, the SAM was decomposed in the irradiated region. The decomposed SAM was further oxidized with active oxygen species generated by photoexcitation of atmospheric oxygen

* To whom correspondence should be addressed.
† Nagoya University.
‡ Aichi Science & Technology Foundation.

10.1021/jp021362r CCC: $25.00
Published on Web 12/28/2002

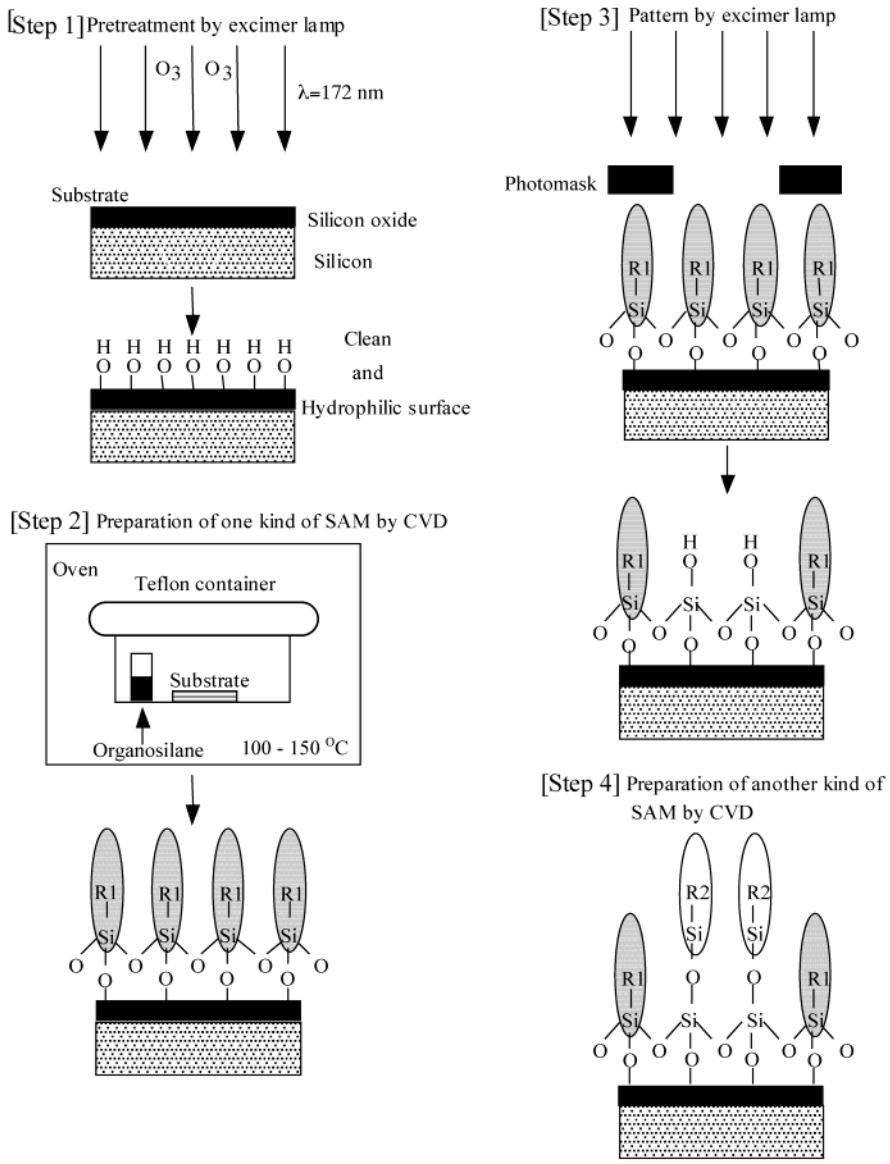

Figure 1. Schematic illustrations of the experimental procedures; preparation of binary-SAM micropatterns.

molecules. Finally, the SAM was removed as volatile species, and thus, the underlying silane oxide layer was exposed. In step 4, another type of SAM was deposited on the photoirradiated region in a similar manner as the step 2. The pattern composed of two types of SAMs was formed on the substrates in this manner.

2.2. FE-SEM Measurement. All of the samples were observed with on FE-SEM (JEOL Ltd., JSM-6300F) under the following conditions: accelerating voltages (V_{acc}) of 0.55−0.70 kV, an emission current of 12×10^{-6} A and a probe current of 1×10^{-11} A. The samples were observed without performing conductive over-coating. Although clear FE-SEM contrasts for the micropatterned SAM samples obtained at V_{acc} around 1 kV or below, image contrasts became faint with an increase in V_{acc}. At $V_{acc} = 5$ kV, there were almost no detectable contrasts. The contrasts did not depended on Vacc (0.55 − 4.0 kV) but the types of SAMs.

2.3. Ab Initio Molecular Orbital Calculations. Ab initio MO calculations were performed using Gaussian 98.[14] The structures and energies were obtained in the hybrid density functional theory with D95 basis set; B3LYP/D95.[15,16] All structural parameters were variable in the optimization. For the MO calculations, we employed model−molecules in which each of the methoxy groups of the organosilane precursors was substituted with a hydrogen atom since these methoxy groups do not remain in the SAMs as illustrated in Figure 1.

3. Results and Discussion

Figure 2 shows FE-SEM images of binary-SAM micropatterns; ODS/AHAPS, AHAPS/CMPhS, and CMPhS/FAS−SAMs. Clear contrasts can be seen between the SAMs in each of the FE−SEM images. Bright regions in ODS/AHAPS, AHAPS/CMPhS, and CMPhS/FAS−SAM samples correspond to the regions covered with ODS, AHAPS, and CMPhS−SAMs, respectively. The order of the contrasts was ascertained as follows:

$$\text{(Bright) ODS−SAM} > \text{AHAPS−SAM} > \text{CMPS−SAM} > \text{FAS−SAM (Dark)} \quad (3)$$

The brightness means that the amounts of emitted secondary electrons in the region were greater than the other region. AHAPS−SAM most readily releases electrons. There is a discrepancy in part between the order of surface potential and that of secondary electron emission. The order of surface potential between ODS and AHAPS−SAMs is in the inverse

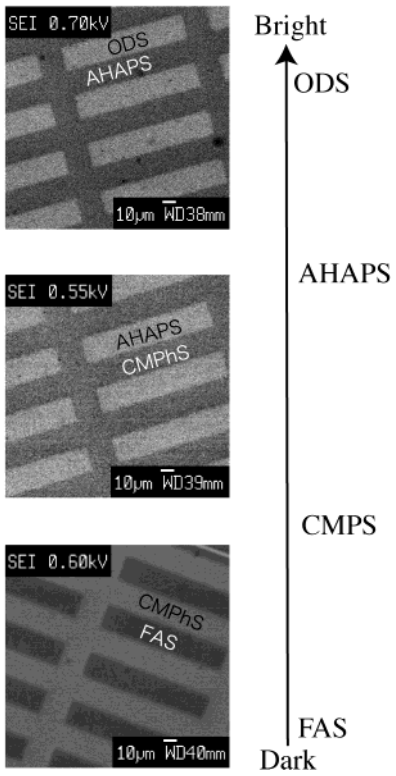

Figure 2. FE−SEM images of binary-SAM micropatterns; ODS/AHAPS, AHAPS/CMPhS, and CMPhS/FAS.

relation with that of the FE−SEM contrasts (see the eq 1). This indicates that the FE−SEM contrasts cannot be explained by the difference of Fermi energy which governs the surface potentials.

To elucidate the origin of the FE−SEM contrasts, we examined the highest occupied and lowest unoccupied molecular orbitals (HOMO and LUMO) of the SAM−molecules. Figure 3 shows drawings of the HOMO and LUMO of the ODS, FAS, AHAPS, and CMPhS−molecules. The HOMO (−0.34059 hartree) and LUMO (−0.07242 hartree) of the FAS-molecule are mainly composed of σ_{Si-C} and σ_{C-F}*, respectively. FAS−molecule has the lower LUMO and HOMO so that these low energy levels lead to the lowest Fermi level (−0.20651 hartree). The HOMO (−0.20447 hartree) and LUMO (0.05042 hartree) of AHAPS−molecule are mainly composed of a lone pair on nitrogen and σ_{Si-C}*, respectively. This lone pair lifts up the energy level of HOMO. The HOMO (−0.27729 hartree) and LUMO (0.05301 hartree) of ODS−molecule are mainly composed of σ_{C-C} and σ_{Si-C}*. ODS−molecule has the highest LUMO among the SAM−molecules used in this study. The HOMO (−0.26128 hartree) and LUMO (−0.05405 hartree) of CMPhS−molecule mainly were composed of $\pi_{C=C}$ and $\pi_{C=C}$*, respectively. CMPhS−SAM has a little stabilization energy originated from the interaction between $\sigma_{C=C}$ and σ_{C-Cl}*. These orbitals do not directly interact with one another but interact with a specific lone pair of chlorine. The little stabilization lowers the Fermi level slightly. Consequently, the Fermi levels of ODS, FAS, AHAPS, and CMPS−molecule become −0.11214, −0.20651, −0.07703, and −0.15767 hartree, respectively. The order of the Fermi levels is summarized as follows.

Fermi levels:

$$\text{(High) AHAPS−molecule} > \text{ODS−molecule} > \text{CMPS−molecule} > \text{FAS−molecule (Low)} \quad (4)$$

This Fermi level order of model molecules decidedly agrees with the order of the surface potentials of the SAMs. However, it does not agree with the order of the brightness in the FE-SEM images. Here, we explain them from the viewpoint of HOMO or LUMO energy levels. The HOMO and LUMO energy levels are related to first ionization potential and electron affinity, respectively. The orders of HOMO and LUMO energy levels are summarized as follows.

HOMO energy levels:

$$\text{(High) AHAPS−SAM} > \text{CMPS−SAM} > \text{ODS−SAM} > \text{FAS−SAM (Low)} \quad (5)$$

LUMO energy levels:

$$\text{(High) ODS−SAM} > \text{AHAPS−SAM} > \text{CMPS−SAM} > \text{FAS−SAM (Low)} \quad (6)$$

Only the LUMO level order agrees with that of the brightness in FE−SEM. We proposed a model of secondary electron emission from SAM as shown in Figure 4. In FE−SEM, primary electrons incident in the SAM and consecutively excite the SAM−molecules. Most electrons in the ground state of each

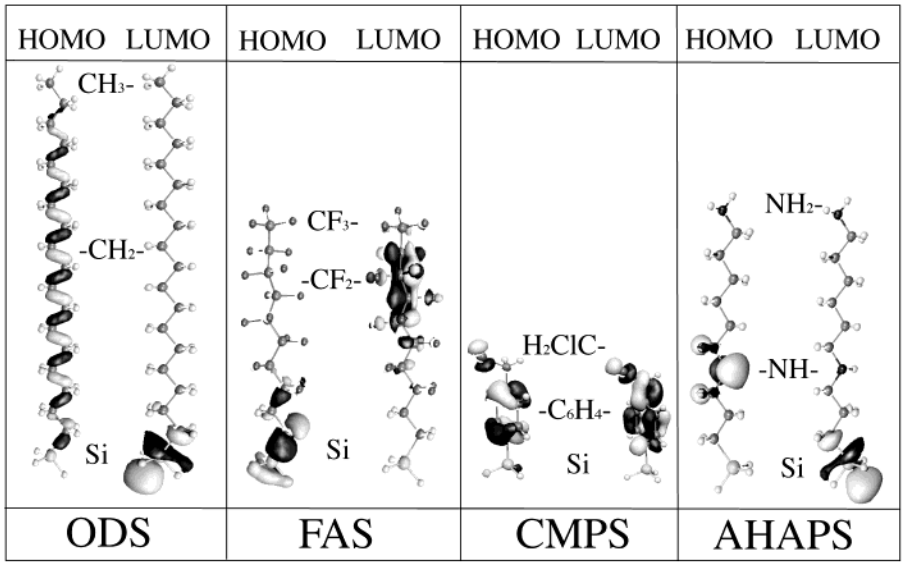

Figure 3. Drawings of the HOMO and LUMO of the ODS, FAS, AHAPS, and CMPhS calculated by B3LYP/D95.

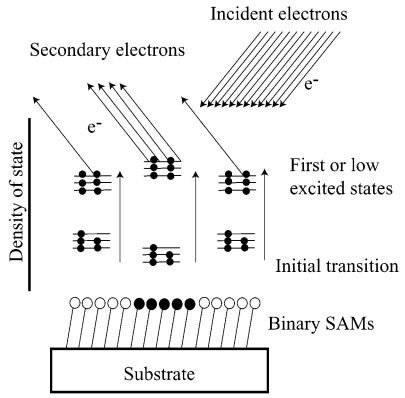

Figure 4. Model to explain the FE−SEM contrasts of binary-SAM maicropatterns.

molecule are excited into first or low excited states of the molecule. The first and low excited states are mainly attributed to the transitions from the HOMO to LUMO bands. Primary electrons further stimulate the SAM molecules resulting in electron emission from the LUMO band as secondary electrons. Thus, a molecule with a higher LUMO level is thought to more readily emit secondary electrons, to the vacuum level. This model can be applied to the FE−SEM contrast because of the higher molecular packing density became brighter in FE−SEM images. When the molecular packing density increases, the density of state, consequently, the number of excited electrons to the LUMO band during FE−SEM observation, increases, resulting in the increase in the amount of secondary electron emission.

4. Conclusion

The micropatterns composed of two different types of organosilane SAMs were clearly observed by FE−SEM. The brightness of the SAMs in FE-SEM was the order of ODS > AHAPS > CMPhS > FAS. The origins of these image contrasts were confirmed to be primarily governed by the LUMO levels of the molecules consisting of the SAMs. FE−SEM is a powerful tool for characterization of micropatterned SAMs. In addition to the ability to observe microstructures, the method has a capability to obtain chemical information through detecting electronic states of molecules on a solid support.

Acknowledgment. This research has been supported by the Research Project "Biomimetic Materials Processing" (No. JSPS-RFTF 99R13101), Research for the Future (RFTF) Program, Japan Society for the Promotion of Science, and by Grant-in-Aid for Scientific Research from the Ministry of Education, Culture, Sports, Science and Technology.

References and Notes

(1) Ulman, A. *An Introduction to Ultrathin Organic Films*; Academic Press: Boston, MA, 1991.

(2) Kumar, A.; Abbott, N. L.; Kim, E.; Biebuyck, H. A.; Whitesides, G. M. *Acc. Chem. Res.* **1995**, *28*, 219−226.

(3) Bishop, A.; Nuzzo, R. G. *Curr. Opin. Colloid Interface Sci.* **1996**, *1*, 127−136.

(4) Ulman, A. *Chem. Rev.* **1996**, *96*, 1533−1554.

(5) Bar, G.; Rubin, S.; Taylor, T. N.; Swanson, B. I.; Zawodzinski, T. A.; Chow, J. T.; Ferraris, J. P. *J. Vac. Sci. Technol. A* **1996**, *14*, 1794−1800.

(6) Xia, Y.; Qin, D.; Yin, Y. *Curr. Opin. Colloid Interface Sci.* **2001**, *6*, 54−64.

(7) Hayashi, K.; Sugimura, H.; Takai, O. *Jpn. J. Appl. Phys. Part 1* **2001**, *40*, 4344−4348.

(8) Fujihira, M. *Annu. Rev. Mater. Sci.* **1999**, *29*, 353−380.

(9) Saito, N.; Hayashi, K.; Sugimura, H., Takai, O.; Nakagiri, N. *Chem. Phys. Lett.* **2001**, *349*, 172−176.

(10) Saito, N.; Hayashi, K.; Sugimura, H.; Takai, O.; Nakagiri, N. *Surf. Interface Anal.* **2002**, *34*, 601−605.

(11) Bittermann, A. G.; Jacobi, S.; Chi, L. F.; Fuchs, H.; Reichelt, R. *Langmuir* **2001**, *17*, 1872−1877.

(12) Hozumi, A.; Ushiyama, K.; Sugimura, H.; Takai, O. *Langmuir* **1999**, *15*, 7600−7604.

(13) Sugimura, H.; Hozumi, A.; Kameyama, T.; Takai, O. *Surf. Interface Analsis*, **2002**, *34*, 550−554.

(14) Frisch, M. J.; Trucks, G. W.; Schlegel, H. B.; Scuseria, G. E.; Robb, M. A.; Cheeseman, J. R.; Zakrzewski, V. G.; Montgomery, J. A., Jr.; Stratmann, R. E.; Burant, J. C.; Dapprich, S.; Millam, J. M.; Daniels, A. D.; Kudin, K. N.; Strain, M. C.; Farkas, O.; Tomasi, J.; Barone, V.; Cossi, M.; Cammi, R.; Mennucci, B.; Pomelli, C.; Adamo, C.; Clifford, S.; Ochterski, J.; Petersson, G. A.; Ayala, P. Y.; Cui, Q.; Morokuma, K.; Malick, D. K.; Rabuck, A. D.; Raghavachari, K.; Foresman, J. B.; Cioslowski, J.; Ortiz, J. V.; Stefanov, B. B.; Liu, G.; Liashenko, A.; Piskorz, P.; Komaromi, I.; Gomperts, R.; Martin, R. L.; Fox, D. J.; Keith, T.; Al-Laham, M. A.; Peng, C. Y.; Nanayakkara, A.; Gonzalez, C.; Challacombe, M.; Gill, P. M. W.; Johnson, B. G.; Chen, W.; Wong, M. W.; Andres, J. L.; Head-Gordon, M.; Replogle, E. S.; Pople, J. A. *Gaussian 98*, revision A.9; Gaussian, Inc.: Pittsburgh, PA, 1998.

(15) Dunning, T. H.; Hay, P. J. In *Modern Theoretical Chemistry*; Schaefer, H. F., Ed.; Plenum: New York, 1976; Vol. 3., 1−28.

(16) Becke, A. D. *J. Chem. Phys.* **1993**, *98*, 5648−5652.